Possibility for an infrared sounder as IASI to document the HCOOH chemistry in biomass burning plumes

Matthieu Pommier[1,*], Cathy Clerbaux[1,2], Pierre-Francois Coheur[2]

1 LATMOS/IPSL, UPMC Univ. Paris 06 Sorbonne Universités, UVSQ, CNRS, Paris, France
2 Spectroscopie de l'Atmosphère, Chimie Quantique et Photophysique, Université Libre de Bruxelles (ULB), Brussels, Belgium
*now at: Norwegian Meteorological Institute, Oslo, Norway

Correspondence to: Matthieu Pommier (matthieup@met.no)

Abstract. Formic acid (HCOOH) concentrations are often underestimated by models and its chemistry is highly uncertain. HCOOH is, however, among the most abundant atmospheric volatile organic compounds and it is potentially responsible for rain acidity in remote areas. HCOOH data from the Infrared Atmospheric Sounding Interferometer (IASI) are analyzed from 2008 to 2014, to estimate enhancement ratios from biomass burning emissions over seven regions. Fire-affected HCOOH and CO total columns are defined by combining total columns from IASI, geographic location of the fires from MODerate resolution Imaging Spectroradiometer (MODIS) and the surface wind speed field from the European Centre for Medium-Range Weather Forecasts (ECMWF). Robust correlations are found between these fire-affected HCOOH and CO total columns over the selected biomass burning regions, allowing the calculation of enhancement ratios equal to $7.30\times10^{-3}\pm0.08\times10^{-3}$ mol/mol over Amazonia, $11.10\times10^{-3}\pm1.37\times10^{-3}$ mol/mol over Australia, $6.80\times10^{-3}\pm0.44\times10^{-3}$ mol/mol over India, $5.80\times10^{-3}\pm0.15\times10^{-3}$ mol/mol over Southern East Asia, $4.00\times10^{-3}\pm0.19\times10^{-3}$ mol/mol over Northern Africa, $5.00\times10^{-3}\pm0.13\times10^{-3}$ mol/mol over Southern Africa, and $4.40\times10^{-3}\pm0.09\times10^{-3}$ mol/mol over Siberia, in a fair agreement with previous studies. The comparison with other studies highlights a possible underestimation by 60% of emission or a secondary production of HCOOH by Siberian forest fires while the studied fire plumes originating from Southern African savanna could suggest a limited secondary production of HCOOH or a limited sink. In comparison with data set characterizing emissions, it is also shown that the selected agricultural burning plumes captured by IASI over India and Southern East Asia correspond to recent plumes where the chemistry or the sink do not occur.

1. Introduction

Formic acid (HCOOH) is one of the most abundant carboxylic acids present in the atmosphere. HCOOH is mainly removed from the troposphere through wet and dry deposition, and to a lesser extent by the OH radical. It is a relatively short-lived species with an average lifetime in the troposphere of 3–4 days (Paulot et al., 2011; Stavrakou et al., 2012). HCOOH contributes for a large fraction to acidity in precipitation in remote areas (e.g. Andreae et al., 1988).

HCOOH is mainly a secondary product from other organic precursors. The largest global source of HCOOH is biogenic and follows the emissions of isoprene, monoterpenes, other terminal alkenes (e.g., Neeb et al., 1997; Lee et al., 2006; Paulot et al., 2011), alkynes (Hatakeyama et al., 1986; Bohn et al., 1996), and acetaldehyde (Andrews et al., 2012; Clubb et al., 2012). There are also small direct emissions by vegetation (Keene and Galloway, 1984, 1988; Gabriel et al., 1999) and biomass burning (e.g. Goode et al., 2000). Other studies highlighted the existence of other sources as from ants (Graedel and Eisner, 1988), dry savanna soils (Sanhueza and Andreae, 1991), motor vehicles (Kawamura et al., 1985; Grosjean, 1989), abiological formation on rock surfaces (Ohta et al., 2000) and cloud processing (Chameides et al., 1983). Their contributions are very uncertain and most are probably minor.

More generally there are still large uncertainties on the sources and sinks of HCOOH, and on the relative contribution of anthropogenic and natural sources, despite the fact that recent progress has been made possible by using the synergy between

45   atmospheric models and satellite data (e.g. Stavrakou et al., 2012; Chaliyakunnel et al., 2016). These uncertainties have an impact on our understanding of the HCOOH tropospheric chemistry, as on the oxidizing power of the atmosphere or the origin of the acid rains. One of the large uncertainties in the HCOOH tropospheric budget seems to be the underestimation of the emissions from the forest fires, as recently suggested by Stavrakou et al. (2012), Cady-Pereira et al. (2014) and Chaliyakunnel et al (2016).

50   One way to estimate the atmospheric emissions of pyrogenic species is the use of emission factors. The emission factors are often obtained from ground and airborne measurements or from small fires burned under controlled laboratory conditions. The emission factors can also be derived from enhancement ratios of the target species relative to a reference species, which is often carbon monoxide (CO) or carbon dioxide (CO_2) due to their long lifetime (e.g. Hurst et al., 1994) and are based on the characteristic of the combustible and hence depends on the type of biomass burning. However, the difference between an

55   emission ratio and an enhancement ratio is that emission ratios are calculated from measurements at the time of emission and enhancement ratios are related to the ongoing chemistry. To correctly convert these enhancement ratios to emission ratios, the decay of the chemical species need to be taken into account or assumptions need to be made, suggesting that the enhancement ratios are equivalent to emission ratios, hence measured at the source and not impacted by chemistry.

Compilations of numerous enhancements ratios, emission ratios and emission factors for several trace gases from

60   measurements at various locations in the world are published regularly (e.g. Akagi et al., 2011) in order to facilitate their use in Chemistry Transport Models.

There has been a recent interest in calculating enhancement ratios and emission factors from satellite data (e.g. Rinsland et al., 2007; Coheur et al., 2009; Tereszchuk et al., 2011). Related to the above difficulty of inferring emission factors using the satellite observations comes from the fact that these observations are indeed typically made in the free/upper troposphere and

65   further downwind of the fires. The fact that satellite mainly probe transported plumes where chemistry modifies the original composition explains why the use of enhancement ratio is more relevant than emission ratio.

Only a few papers have reported on the use of satellite retrievals to study tropospheric HCOOH as with the nadir-viewing Infrared Atmospheric Sounding Interferometer (IASI) (e.g. Stavrakou et al., 2012; R'Honi et al., 2013; Pommier et al., 2016), and with the Tropospheric Emission Spectrometer (TES) (e.g. Cady-Pereira et al., 2014; Chaliyakunnel et al., 2016).

70   Other studies have used the solar occultation Atmospheric Chemistry Experiment (ACE-FTS) which measures the atmospheric composition in the upper troposphere (e.g. Rinsland et al., 2006; Tereszchuk et al., 2011; 2013) and the Michelson Interferometer for Passive Atmospheric Sounding (MIPAS) limb instrument which is sensitive to around 10 km (Grutter et al., 2010).

These Infrared (IR) sounders have limited vertical sensitivity as compared to the ground-based or airborne measurements but

75   their spatial coverage represents a major advantage, which allows observing remote regions which are sparsely studied by field measurements, like the biomass burning regions.

This work aims to provide a list of enhancement ratios relative to CO for HCOOH over several biomass burning regions. For this, we analyzed seven years of IASI measurements, between 2008 and 2014. Section 2 describes the IASI satellite mission and the retrieval characteristics for the CO and the HCOOH total columns. Section 3 presents the fire product used from the

80   MODerate resolution Imaging Spectroradiometer (MODIS) to identify the fire locations. Section 4 details the methodology used to identify of the IASI fire-affected observations. In Section 5 we describe and analyze the enhancements ratios obtained from the IASI measurements and we compare these values to those available in the literature. Finally, the conclusions are presented in Section 6.

2. HCOOH and CO columns from IASI

2.1 The IASI mission

IASI is a nadir-viewing Fourier Transform Spectrometer. Two models are currently in orbit. The first model (IASI-A), was launched onboard the METOP-A platform in October 2006. The second instrument was launched in September 2012 onboard METOP-B. Owing to its wide swath, IASI delivers near global coverage twice per day with observation at around 09:30 and 21:30 local time. Each atmospheric view is composed of 2×2 circular pixels with a 12 km footprint diameter, spaced out by 50 km at nadir. IASI measures in the thermal infrared part of the spectrum, between 645 and 2760 cm^{-1}. It records radiance from the Earth's surface and the atmosphere with an apodized spectral resolution of 0.5 cm^{-1}, spectrally sampled at 0.25 cm^{-1}. IASI has a wavenumber-dependent radiometric noise ranging from 0.1 to 0.4K for a reference blackbody at 280K (Clerbaux et al., 2009), and more specifically around 0.15K for HCOOH and 0.20K for the CO the spectral ranges (~1105 cm^{-1} and ~2150 cm^{-1}, respectively).

The HCOOH and CO columns from IASI are used hereafter to determine the enhancement ratios of HCOOH. CO is chosen as reference due to its longer tropospheric lifetime (several weeks) as compared to HCOOH. In our study we use CO as the reference and not CO_2 since variations in CO_2 concentration are difficult to measure with sufficient accuracy from IASI.

2.2 The CO retrieval characteristics

The CO concentrations are retrieved from IASI using the FORLI-CO software (Hurtmans et al., 2012), which uses an optimal estimation method based on Rodgers (2000). The spectral range used for the retrieval is between 2143 and 2181.25 cm^{-1}. The CO total columns have been validated for different locations and atmospheric conditions (e.g. De Wachter et al., 2012; Kerzenmacher et al., 2012) and the comparison with other data have shown good agreement overall, even if some discrepancies were found within CO-enriched plumes (reaching 12% over the Arctic in summer, see Pommier et al, 2010; and reaching 17% in comparison with other IR sounders, see George et al., 2009). These data were also used previously to study the biomass burning plumes (e.g. Turquety et al., 2009; Pommier et al, 2010; Krol et al., 2013; Whitburn et al., 2015). In order to keep only the most reliable retrievals, the selected data used have a root-mean-square error lower than 2.7×10^{-9} W/(cm^2 cm^{-1} sr) and a bias ranging between -0.15 and 0.25×10^{-9} as recommended in Hurtmans et al. (2012).

2.3 The HCOOH retrieval characteristics

The retrieval is based on the determination of the brightness temperature difference (ΔT_b) between spectral channels with and without the signature of HCOOH. The reference channels used for the calculation of ΔT_b were chosen on both sides of the HCOOH Q-branch (1105 cm^{-1}), i.e., at 1103.0 and 1109.0 cm^{-1}. These ΔT_b were converted into total columns of HCOOH using conversion factors compiled in look-up tables. This simple and efficient retrieval method is described in more details in Pommier et al. (2016).

As shown in Pommier et al. (2016), the vertical sensitivity of the IASI HCOOH total column ranges between 1 and 6 km. This study also showed that large HCOOH total columns were detected over biomass burning regions (e.g. Africa, Siberia) even if the largest values were found to be underestimated. This underestimation, which is lower than 35% for the columns below 2.5×10^{16} molec/cm^2 (Pommier et al., 2006), will propagate in the enhancement ratios calculated in this work.

On the other hand, a large overestimation of the IASI HCOOH columns was shown in comparison with ground-based FTIR. This overestimation was larger for background columns (expected to reach 80% for a column close to 0.3×10^{16} molec/cm^2) and it can also impact our enhancement ratios.

3. MODIS

To identify the fire locations (hotspot), the fire product from the MODerate resolution Imaging Spectroradiometer (MODIS) on board the polar orbiting sun-synchronous NASA Terra and Aqua satellites (Justice et al., 2002; Giglio et al., 2006) are
125 used. The Terra and Aqua satellites equatorial overpass times are ~10:30 and ~13:30 local time, respectively. Fire pixels are 1 km×1 km in size at nadir.

For this work, we use more specifically, the Global Monthly Fire Location Product (MCD14ML, Level 2, Collection 5) developed by the University of Maryland (https://earthdata.nasa.gov/data/near-real-time-data/firms/active-fire-data#tab-content-6) which for each detected fire pixel includes, the geographic location of the fire, the fire radiative power (FRP), the
130 confidence in detection, and the acquisition date and time. The FRP provides a measure of fire intensity that is linked to the fire fuel consumption rate (e.g. Wooster et al., 2005).

Only data presenting a high confidence percentage are used, i.e. higher or equal than 80% as recommended in the MODIS user's guide (Giglio, 2013).

4. Identifying fire-affected IASI observations

135 ### 4.1 The selected areas

The determination of the biomass burning regions is based on the MODIS fire product. Figure 1 highlights the main areas that contributed to the biomass burning for the period between 2008 and 2014. Seven regions were selected for this work: Amazonia (AMA, 5-15°S 40-60°W), corresponding mainly to the Brazilian Cerrado, Australia (AUS, 12-15°S 131-135°E), Northern Africa (NAF, 3-10°N 15-30°E), Southern Africa (SAF, 5-10°S 15-30°E), Southern East Asia (SEA, 18-27°N 96-
140 105°E), India (IND, 15-27°N 75-88°E) and Siberia (SIB, 55-65°N 80-120°E). Among these regions, India and Siberia were not the most actives in terms of number of fires but it seemed important to also investigate them. One first reason for this is that Pommier et al. (2016) showed a misrepresentation of the fire emissions of HCOOH over India. Secondly, India also encounters excess of acidity in rainwater, which could be partly attributed to biomass burning (e.g. Bisht et al., 2014). Concerning Siberia, this region and the surrounding areas experienced intense fires over the past years such as during the
145 summer 2010 (Pommier et al., 2016; and R'honi et al. 2013 for the region close to Moscow).

4.2 The IASI data used

For this work, both the daytime and nighttime IASI data were used. We have verified that using only the daytime retrievals did not change the results. Figure 2 presents the time-series of the monthly mean for the HCOOH and CO total columns over the seven selected regions. The number of fires and their FRP are also indicated. The variation in the total columns of
150 HCOOH and CO matches relatively well with the variation of the number of fires. It is also worth noting that these variations in the total columns do not depend on the intensity of the fires as shown by Fig. 2 and by the scatterplots with the values characterizing each fire as described below (not shown).

The monthly HCOOH and CO total columns are found to be highly correlated over the selected biomass burning regions (correlation from 0.75 to 0.91), except over India (r=0.34) and Siberia (r=0.58). Over both regions, the impact of other
155 sources than biomass burning is thus not negligible. Over India, the CO budget is influenced by long-range transport (e.g. Srinivas et al., 2016) and the anthropogenic emissions have also a large impact (e.g. Ohara et al., 2007). This could explain that the variation in CO does not follow perfectly the variation in the number of fires and that the difference between the background level and the CO peaks is less marked than for the HCOOH. Over Siberia, a temporal shift between the highest peaks for CO and for HCOOH is noticed for few years as for 2009, 2010 and 2011. For these years, the variation in CO does
160 not follow the variation in the number of fires. The large selected region over Siberia is known to be also impacted by CO-enriched plumes transported from other regions as by polluted air masses from China (e.g. Paris et al., 2008) or from Europe

(e.g. Pochanart et al., 2003). These external influences interfere with the CO plumes originating from forest fires measured over this region.

Despite the overall good match between the number of fires and the variation in HCOOH and CO, we are not certain that the
165   HCOOH and the CO were emitted solely by fires, and the discrimination between a natural and an anthropogenic origin for each compound is challenging. This assessment is particularly obvious for IND and SIB. To isolate the HCOOH and CO signals measured by IASI, potentially emitted by a fire, we decided to only use the data in the vicinity of each MODIS hotspot. To do so, we co-located the IASI data at 50 km around each MODIS pixel and between 0 and 5h for each detected fire, so that each MODIS pixel is associated with a value of HCOOH and CO total columns from IASI.

170   With these co-location criteria good correlation coefficients, calculated by linear least-square fitting, are found between the HCOOH and the CO total columns as shown in Tab. 1. The lower coefficients, i.e. less than 0.7 are found for India, Australia, Siberia and Northern Africa. It is also important to note that the HCOOH and the CO columns are better correlated for India and Siberia compared to the monthly time-series shown in Fig. 2. The three other regions present a large correlation, around 0.8. The high correlation suggests that IASI sampled the same biomass burning air mass for these
175   compounds.

4.3 Importance of the meteorological conditions

As shown by earlier studies, the wind speed can have a large influence on the detection of tropospheric plumes of trace gases from space (e.g NO$_2$: Beirle et al., 2011; CO: Pommier et al., 2013; SO$_2$: Fioletov et al., 2015). We have chosen to attribute a surface wind speed value for each MODIS hotspot. These meteorological fields were taken from the ECMWF (European
180   Centre for Medium-Range Weather Forecasts) reanalysis data (http://data-portal.ecmwf.int/data/d/interim_full_daily) (Dee et al., 2011). The horizontal resolution of these fields is 0.125° on longitude and latitude with a 6h time step. As shown in Fig 3, the three regions where the HCOOH:CO correlations are found to be high (close to 0.8), correspond to the regions where the surface wind speed was lower, i.e. for AMA, SEA and SAF. IND has also a low mean and median values but the distribution of the surface wind speed is more spread out than for these three regions.

185   When filtering out the data associated with a large surface wind (higher than 1.44 m/s), new correlations between the HCOOH and the CO total columns from IASI are calculated (Tab. 2). This value of 1.44 m/s for the surface wind speed corresponds to the 25th percentile of the distribution of the three regions characterized by the lowest surface wind speed (Fig. 3).

The correlation coefficients, shown on the scatterplots in Fig. 4 and summarized in Tab. 2, increase for all regions except
190   over NAF, where the coefficient is found to be slightly lower than the previous correlation (Tab. 1). The correlation coefficient is significantly improved over IND and SIB (Tab. 2). These results confirm a robust correlation between the HCOOH and the CO total columns measured by IASI in the vicinity of each MODIS fire location.

5. Analysis of the data over the fire regions

5.1. Determination of the enhancement ratios

195   Based on scatterplots in Fig. 4, an enhancement ratio can be calculated for each region. These enhancement ratios defined as ER$_{(HCOOH/CO)}$, correspond to the value of the slope $\partial[HCOOH]/\partial[CO]$ found in Fig 4. This technique to determine the ER$_{(HCOOH/CO)}$ is more reliable than to only use the columns themselves, i.e. by estimating an ER$_{(HCOOH/CO)}$ for each measurements pairs (HCOOH, CO). Indeed, to perform scatterplots helps to identify a common origin for HCOOH and CO. The values of the ER$_{(HCOOH/CO)}$ over each region are summarized in Tab. 3.

200 It is known that trace gas concentrations within smoke plumes can vary rapidly with time and are very sensitive to chemistry, so a comparison with previous works is always challenging, especially if these studies were performed in another altitude range, at a different location or period of the year.

A good agreement is however globally found with previous studies even if it is important to keep in mind that an underestimation of our $ER_{(HCOOH/CO)}$ is possible due to the underestimation in the highest values of HCOOH as over the

205 forest fires (see Section 2.3). On the other hand, the overestimation of the background column can also impact the calculation of our $ER_{(HCOOH/CO)}$. Both biases is however limited since most of HCOOH total columns used in our analysis over the selected regions are higher than 0.3×10^{16} molec/cm^2 and lower than 2.5×10^{16} molec/cm^2 as explained in Section 2.3. Nevertheless, in order to investigate the possible impact of the overestimation in the lower columns on the calculated ratio, a test was performed, by using only HCOOH columns with a thermal contrast larger than 10K. Indeed, the increase in the

210 thermal contrast (i.e. the temperature difference between the surface and the first layer in the retrieved profile) leads to improve the detection limit and thus to minimize the bias with the lowest columns, as shown in Pommier al. (2016). Similar results were generally found in terms of slope and correlation coefficient, suggesting a negligible effect of the low column biases. The only exception being an increase in $ER_{(HCOOH/CO)}$ over Siberia ($6.5 \times 10^{-3} \pm 0.19 \times 10^{-3}$ mol/mol against 4.4×10^{-3} mol/mol $\pm 0.09 \times 10^{-3}$ in tab. 3). This gives us confidence that the results presented in Tab. 3 are reliable.

215 When compared with other studies, the best agreement for the values presented in Tab. 3 is found over Southern Africa where the $ER_{(HCOOH/CO)}$ ($5 \times 10^{-3} \pm 0.13 \times 10^{-3}$ mol/mol) is similar to the value calculated by Vigouroux et al. (2012) and Coheur et al. (2007). It also agrees with the broad range of values of emission ratios ($EmR_{(HCOOH/CO)}$) referenced by Sinha et al. (2003). This result reinforces the relevance of the methodology used in this work over this region for the identification of the fire-affected IASI columns close to the source. Vigouroux et al. (2012) sampled biomass burning outflow of Southern

220 Africa, Coheur et al. (2007) calculated their $ER_{(HCOOH/CO)}$ in plumes observed over Tanzania in the upper troposphere while Sinha et al. (2003) did it within plumes over Zambia at the origin of the fire. A few assumptions can be given but the analysis given hereafter is only indicative since these previous studies did not measure the same plume than those presented in this work and our $ER_{(HCOOH/CO)}$ is calculated without making any distinction on the seasonal variation or on the type of biomass burning plumes sampled (e.g. emitted by a savanna fire or by a forest fire). Since these $ER_{(HCOOH/CO)}$ from previous

225 studies and the $EmR_{(HCOOH/CO)}$ from Sinha et al. (2003) agree with our $ER_{(HCOOH/CO)}$, and since HCOOH has a short lifetime, this may suggest that the selected plumes measured by IASI from 2008 to 2014 and those sampled by Vigouroux et al. (2012) and Coheur et al. (2007), encountered a limited secondary production or a low sink as deposition or reaction with OH in the troposphere during their transport. Moreover, the decay of HCOOH is faster than for CO, suggesting that these plumes are rapidly advected in the troposphere. Our $ER_{(HCOOH/CO)}$ differs however from the value in Rinsland et al. (2006) (11.3×10^{-3}

230 $\pm 7.6 \times 10^{-3}$ mol/mol) since our ratio is 55% lower. One possible explanation is the multi-origin of the plumes studied by Rinsland et al. (2006), since, based on their backward trajectory, their plumes could be influenced by biomass burning originating from Southern Africa and/or from Southern America. It is worth noting the ACE-FTS instrument used in their study, works in a limb solar occultation mode. This means the atmospheric density sampled by the instrument is larger than the one measured by the nadir geometry as with IASI. However, the difference in geometry is not a reliable assumption in

235 this case, since it is does not explain the reasons of the agreement with the ACE-FTS measurements used by Coheur et al. (2007) and the disagreement with those from Rinsland et al. (2006). The impact of the difference in the geometry of sampling in the HCOOH retrieval needs however to be estimated in a proper comparison between both instruments. Such comparison could also be extended with the difference in the assumptions used in the retrieval (e.g. the a priori). The $ER_{(HCOOH/CO)}$ from our work is also 15% lower than the $EmR_{(HCOOH/CO)}$ in Yokelson et al. (2003) ($5.9 \times 10^{-3} \pm 2.2 \times 10^{-3}$

240 mol/mol). With this difference we can also suggest the presence of a sink of HCOOH within the plumes detected by IASI or this slight underestimation is simply related to the faster decay of HCOOH than the one of CO. In opposite, the $ER_{(HCOOH/CO)}$ retrieved from IASI is also twice higher than the $ER_{(HCOOH/CO)}$ in Chaliyakunnel et al. (2016) ($2.6 \times 10^{-3} \pm 0.3 \times 10^{-3}$ mol/mol).

Chaliyakunnel et al. (2016) developed an approach allowing the determination of pyrogenic $ER_{(HCOOH/CO)}$ by reducing the impact of the mix with the ambient air, and they concluded that their most reliable value on the amount of HCOOH produced from fire emissions was obtained for African fires.

Over Northern Africa, the calculated $ER_{(HCOOH/CO)}$ (4×10^{-3} ± 0.19×10^{-3} mol/mol) is 42% higher than the $ER_{(HCOOH/CO)}$ calculated in Chaliyakunnel et al. (2016) (2.8×10^{-3} ± 0.4×10^{-3} mol/mol). It is worth reminding that NAF is the region characterized by a scatterplot with the lowest correlation coefficient (Fig. 4).

A larger difference is found over Australia where the $ER_{(HCOOH/CO)}$ is 11.1×10^{-3} ± 1.37×10^{-3} mol/mol. This $ER_{(HCOOH/CO)}$ is roughly the mean of both values reported by Paton-Walsh et al. (2005) and Chaliyakunnel et al. (2016). The difference between our work and the one done by Paton-Walsh et al. (2005) could maybe be explained by the different origin of the probed plume. In our case, the studied area corresponds to the Northern part of the Northern Territory with savanna-type vegetation while Paton-Walsh et al. (2005) sampled bush fire plumes coming from the Eastern Coast of Australia, representative of Australian temperate forest. In the work done by Chaliyakunnel et al. (2016), a quite uncertain value is reported, with an error larger than their $ER_{(HCOOH/CO)}$.

Over Amazonia, our $ER_{(HCOOH/CO)}$ (7.3×10^{-3} ± 0.08×10^{-3} mol/mol) is similar to the value given in Chaliyakunnel et al. (2016), who report however a larger bias over Amazonia. Over this region, our $ER_{(HCOOH/CO)}$ is higher than the one obtained by González Abad et al. (2009) with ACE-FTS in the upper troposphere (5.1×10^{-3} ± 1.5×10^{-3} mol/mol). This difference with the study done by González Abad et al. (2009) may be explained by the difference in the altitude of the detection of the forest fire plume between IASI (mid-troposphere) and ACE-FTS (upper-troposphere) and thus by a difference in the ongoing chemistry within their respective sampled plumes. The geometry of the sampling (nadir vs limb) or the difference in the retrieval may also have an impact in the retrieved HCOOH.

The Siberian $ER_{(HCOOH/CO)}$ (4.4×10^{-3} mol/mol ± 0.09×10^{-3}) is found to be in good agreement with the wide range of values obtained by Tereszchuk et al. (2013) and Viatte et al. (2015). This $ER_{(HCOOH/CO)}$ is however lower than the ratios calculated by R'Honi et al. (2013) who focused on the extreme fire event that occurred in 2010.

For India and Southern East Asia, the comparison is not possible since no previous studies were reported. The comparison is performed next, based on the emission factors.

5.2. Comparison with emission ratios calculated from the emission factors found in literature

We have complemented our comparison of the enhancement ratios by calculating emissions ratios using emission factors found in literature. The main argument to perform such comparison is the lack of measurements of enhancement ratios over IND and SEA.

Even if our methodology tries to characterize the HCOOH emitted by biomass burning close to the source, our columns are probably not representative of the emission at the origin of the fire. The altitude of the sampling (mid-troposphere) and the age of the plumes (at least a few hours) have a large impact in our enhancement ratios.

To perform a proper comparison with emission ratios, our enhancement ratios should be converted to emission ratios. To do so, it would be essential to take into account the decay of the compounds during the transport of the plume. However, due to the methodology used, i.e. averaging the data collected during a few hours (between 0 and 5h from the time registered by MODIS for each detected fire), the calculation of the decay of each compound is not possible. The comparison presented hereafter is therefore mostly illustrative.

For both, IND and SEA regions, the emission ratios have been calculated from the emission factors provided in Akagi et al. (2011). For the other regions, in addition to the values from Akagi et al. (2011), emission ratios were similarly calculated from emission factors given in other studies.

Based on the emission ratios, the emission factors are usually derived by this following equation:

$$EF_{HCOOH} = EF_{CO} \times MW_{HCOOH}/MW_{CO} \times EmR_{(HCOOH/CO)} \qquad (1)$$

EF_{HCOOH} is the emission factor for HCOOH; $EmR_{(HCOOH/CO)}$ is the molar emission ratio of HCOOH with respect to CO;

285   MW_{HCOOH} is the molecular weight of HCOOH; MW_{CO} is the molecular weight of CO and EF_{CO} is the emission factor for CO for dry matter, set to the value taken from Akagi et al. (2011).

Thus, based on equation (1), $EmR_{(HCOOH/CO)}$ were calculated and compared with our $ER_{(HCOOH/CO)}$. In this calculation, the vegetation type characterizing each region is important. Some regions are composed by a mix of vegetation types. This is the case for example for AMA and SAF (e.g. White, 1981), composed by tropical forest and savanna, characterized by an EF_{CO}

290   of 93±27 g/kg and 63±17 g/kg respectively (Akagi et al., 2011). AUS and NAF correspond to a savanna fuel type. SIB is a boreal forest area with an EF_{CO} of 127±45 g/kg. Based also on the maps shown by Fig. 9 in Schreier et al. (2014) and Fig. 13 in van der Werf, et al. (2010), the soil for IND is supposed to be mainly composed by cropland (agriculture), which is associated to an EF_{CO} of 102±33 g/kg, and probably also by extratropical forest which is characterized with an EF_{CO} equal to 122±44 g/kg. The fuel type for SEA is supposed to be a mix of extratropical forest and savanna, with EF_{CO} of 122±44 g/kg,

295   and 63±17 g/kg, respectively. Cropland fuel type was also used since large agricultural biomass burning is occurring in this region (e.g. Duc et al., 2016).

Despite the assumptions made, a fair agreement is found over Southern Africa. Our $ER_{(HCOOH/CO)}$ ($5 \times 10^{-3} \pm 0.13 \times 10^{-3}$ mol/mol) is indeed similar to the $EmR_{(HCOOH/CO)}$ calculated from Sinha et al. (2004) by using savanna fuel type and the $ER_{(HCOOH/CO)}$ is between both values calculated from Yokelson et al. (2003). This agreement is consistent since both previous

300   studies sampled plumes emitted by savanna fires. Yokelson et al. (2003) and Sinha et al. (2004) used also both the same sampling strategy. They sampled fire plumes by penetrating several minutes old plumes at relatively low altitude (up to 1.3 km for Sinha et al. (2004) and just above the flame front for Yokelson et al. (2003)). This agreement shows, as already described in the previous section, our $ER_{(HCOOH/CO)}$ over Southern Africa is similar to their $EmR_{(HCOOH/CO)}$. On other hand, it is worth noting that our $ER_{(HCOOH/CO)}$ is also similar to the $EmR_{(HCOOH/CO)}$ from Akagi et al. (2011) but for the tropical forest.

305   A large underestimation compared to Rinsland et al. (2006) is found. This underestimation confirms the disagreement with this study already shown in Tab. 3.

Over Northern Africa, our $ER_{(HCOOH/CO)}$ is twice larger than the value provided by Akagi et al. (2011), probably due to the lower correlation found in our scatterplot. This is highly probable that our presumed fire-affected IASI columns are indeed impacted by other air masses.

310   For Amazonia, the calculated $ER_{(HCOOH/CO)}$ ($7.3 \times 10^{-3} \pm 0.08 \times 10^{-3}$ mol/mol) is close to the value given in Akagi et al. (2011) for the tropical forest (5.2×10^{-3} mol/mol), but it is three times higher than the values derived from Yokelson et al. (2007; 2008) for the same vegetation type. For the latter, it is worth noting that their factors have been corrected a posteriori (scaled down by a factor of 2.1), as described in their comment following the paper done by R'Honi et al. (2013) (see Yokelson et al., 2013). As Yokelson et al. (2007; 2008) sampled the forest fires plumes by penetrating recent columns of smoke 200–

315   1000m above the flame front, our $ER_{(HCOOH/CO)}$ may reflect a secondary production of HCOOH. This assuming secondary production is less substantial by comparing with the value from Akagi et al. (2011).

Over Australia and over Siberia, the calculated $ER_{(HCOOH/CO)}$ is overestimated compared to the values given in Akagi et al. (2011) for a savanna fire and for a boreal forest, respectively. If our value for near-source estimation is correct, this would probably mean that the direct emission is underestimated (by 450% over Australia and by 60% over Siberia) or that a large

320   secondary production of HCOOH from Australian and Siberian fires occurred. Over Australia the difference is very large even if it is worth noting that the comparison done by Pommier al. (2016) with FTIR measurements showed the lowest bias was for the Australian site (-2% at Wollongong).

Finally, in this comparison, the studied plumes over India and Southern East Asia are certainly related to agricultural fires. This is strongly possible as agricultural residue burning is prevalent in these regions (e.g. Kaskaoutis et al., 2014; Vadrevu et

325   al., 2015). Over India and over Southern East Asia, our $ER_{(HCOOH/CO)}$ ($6.8 \times 10^{-3} \pm 0.44 \times 10^{-3}$ mol/mol for India and $5.8 \times 10^{-3} \pm$

0.15×10^{-3} mol/mol for Southern East Asia) are close to the value referenced by Akagi et al. (2011) for cropland fires (6×10^{-3} mol/mol). Since our $ER_{(HCOOH/CO)}$ are close to the $EmR_{(HCOOH/CO)}$ derived from the EF_{HCOOH} in Akagi et al. (2011), this may suggests the studied plumes gathered along the 7-yr period correspond to fresh plumes where the chemistry or the sink do not occur.

6. Conclusions

Seven years of HCOOH data measured by IASI over seven different fire regions around the world were analyzed (AMA=Amazonia, AUS=Australia, IND = India, SEA = Southern East Asia, NAF= Northern Africa, SAF= Southern Africa, SIB= Siberia). By taking into account the surface wind speed and by characterizing each MODIS fire hotspot with a value of HCOOH and CO total columns, this work established enhancement ratios for the seven biomass burning areas and compared them to reported values found in literature.

The difficulties in performing such comparison is associated with the difference in locations, the difference in the altitude of the sampling and the difference in age of each fire plume studied in previous publications. A fair agreement was however found for the enhancement ratios calculated in this work, in comparison with other studies, using satellite or airborne or FTIR measurements.

In agreement with previous studies, the plumes from Southern African savanna fires may reflect a limited secondary production or a limited sink occurring in the upper layers of the troposphere during their transport. Such assumptions remain however difficult to make by comparing individual plumes (from previous studies) with plumes gathering during a 7-yr period (from IASI). Plumes from agricultural fires over India and Southern East Asia probably correspond to fresh plumes as our $ER_{(HCOOH/CO)}$ based on the 7-yr IASI measurements are similar to the $EmR_{(HCOOH/CO)}$ calculated from emission factors provided by Akagi et al. (2011).

A very good agreement was found over Amazonia, especially with the work done by Chaliyakunnel et al. (2016) who determinated pyrogenic $ER_{(HCOOH/CO)}$.

Fires over Australia and over Siberia are probably underestimated in terms of direct emission or secondary production of HCOOH. The analysis over Australia is however delicate as our $ER_{(HCOOH/CO)}$ approximately corresponds to the mean of the values reported in Paton-Walsh et al. (2005) and in Chaliyakunnel et al. (2016); and it is also 450% higher than the $EmR_{(HCOOH/CO)}$ derived from Akagi et al. (2011). The underestimation by 60% over Siberia is consistent with conclusions given in R'Honi et al. (2013).

Finally, the values found over Northern Africa were the more difficult to interpret as this region is characterized by the poorer correlation between our fire-affected HCOOH and CO total columns.

With these findings and by updating the enhancement ratios, an interesting modeling work could be performed to estimate a new tropospheric budget for HCOOH. This IASI data set may also be used in the future to study a single plume at different time. This would be useful for the characterization of the chemistry ongoing in a fire plume outflow.

An inter-comparison with other space-borne instruments as TES and ACE-FTS will be helpful to interpret the difference and the biases between the retrieved HCOOH columns in thus between their respective $ER_{(HCOOH/CO)}$.

7. Data availability

The IASI FORLI CO products are publicly available via the Aeris data infrastructure (http://www.aeris-data.fr/) while the IASI HCOOH columns will be made available soon through the same platform.

Acknowledgments

The IASI mission is a joint mission of EUMETSAT and the Centre National d'Etudes Spatiales (CNES, France). The IASI L1 data are distributed in near real time by EUMETSAT through the EUMETCast system distribution. We thank the MODIS team for providing public access to fire products MCD14ML. This MODIS data set was provided by the University of
370 Maryland and NASA FIRMS operated by NASA/GSFC/ESDIS with funding provided by NASA/HQ. The authors thank S. Whitburn (ULB) for his help on the MODIS files. They also thank J. Hadji-Lazaro (LATMOS) and L. Clarisse (ULB) for preparing the IASI ΔT_b data set. The authors also acknowledge ECMWF for the free access to the meteorological data.

375 **References**

Akagi, S. K., Yokelson, R. J., Wiedinmyer, C., Alvarado, M. J., Reid, J. S., Karl, T., Crounse, J. D., and Wennberg, P. O.: Emission factors for open and domestic biomass burning for use in atmospheric models, Atmos. Chem. Phys., 11, 4039-4072, doi:10.5194/acp-11-4039-2011, 2011.

380

Andreae, M. O., Andreae, T. W., Talbot, R. W., and Harriss, R. C.: Formic and acetic acid over the central Amazon region, Brazil, I. Dry season, J. Geophys. Res., 93, 1616–1624, doi:10.1029/JD093iD02p01616, 1988.

Andrews, D. U., Heazlewood, B. R., Maccarone, A. T., Conroy, T., Payne, R. J., Jordan, M. J. T., and Kable, S. H.: Photo-
385 tautomerization of acetaldehyde to vinyl alcohol: a potential route to tropospheric acids, Science, 337, 1203–1206, 2012.

Beirle, S., K. F. Boersma, U. Platt, M. G. Lawrence, and T. Wagner : Megacity emissions and lifetimes of nitrogen oxides probed from space, Science, 333, 1737–1739, doi:10.1126/science.1207824, 2011.

390 Bisht, D. S., Tiwari, S., Srivastava, A. K., Singh, J. V., Singh, B. P., Srivastava, M. K. : High concentration of acidic species in rainwater at Varanasi in the Indo-Gangetic Plains, India, Nat Hazards, 75, 2985–3003, DOI 10.1007/s11069-014-1473-0, 2014.

Bohn, B., Siese, M., and Zetzschn, C.: Kinetics of the OH+C_2H_2 reaction in the presence of O_2, J. Chem. Soc. Faraday T.,
395 92, 1459–1466, 1996.

Cady-Pereira, K. E., Chaliyakunnel, S., Shephard, M. W., Millet, D. B., Luo, M., and Wells, K. C.: HCOOH measurements from space: TES retrieval algorithm and observed global distribution, Atmos. Meas. Tech., 7, 2297-2311, doi:10.5194/amt-7-2297-2014, 2014.

400

Chaliyakunnel, S., Millet, D. B., Wells, K. C., Cady-Pereira, K. E., and Shephard, M. W.: A Large Underestimate of Formic Acid from Tropical Fires: Constraints from Space-Borne Measurements, Environ. Sci. Technol., 50, 5631–5640, doi:10.1021/acs.est.5b06385, 2016.

405 Chameides, W. L. and Davis, D. D.: Aqueous-phase source of formic acid in clouds. Nature 304, 427-429, 1983.

Clerbaux, C., Boynard, A., Clarisse, L., George, M., Hadji-Lazaro, J., Herbin, H., Hurtmans, D., Pommier, M., Razavi, A., Turquety, S., Wespes, C., and Coheur, P.-F.: Monitoring of atmospheric composition using the thermal infrared IASI/MetOp sounder, Atmos. Chem. Phys., 9, 6041-6054, doi:10.5194/acp-9-6041-2009, 2009.

410

Clubb, A. E., Jordan, M. J. T., Kable, S. H., and Osborn, D. L.: Phototautomerization of Acetaldehyde to vinyl alcohol: a primary process in UV-irradiated acetaldehyde from 295 to 335nm, J. Phys. Chem. Lett., 3, 3522–3526, 2012.

Coheur, P.-F., Herbin, H., Clerbaux, C., Hurtmans, D., Wespes, C., Carleer, M., Turquety, S., Rinsland, C. P., Remedios, J.,

415   Hauglustaine, D., Boone, C. D., and Bernath, P. F.: ACE-FTS observation of a young biomass burning plume: first reported measurements of C_2H_4, C_3H_6O, H_2CO and PAN by infrared occultation from space, Atmos. Chem. Phys., 7, 5437-5446, doi:10.5194/acp-7-5437-2007, 2007.

Coheur, P.-F., Clarisse, L., Turquety, S., Hurtmans, D., and Clerbaux, C.: IASI measurements of reactive trace species in

420   biomass burning plumes, Atmos. Chem. Phys., 9, 5655-5667, doi:10.5194/acp-9-5655-2009, 2009.

Dee, D. P. and Uppala, S. M. and Simmons, A. J. and Berrisford, P. and Poli, P. and Kobayashi, S. and Andrae, U. and Balmaseda, M. A. and Balsamo, G. and Bauer, P. and Bechtold, P. and Beljaars, A. C. M. and van de Berg, L. and Bidlot, J. and Bormann, N. and Delsol, C. and Dragani, R. and Fuentes, M. and Geer, A. J. and Haimberger, L. and Healy, S. B. and

425   Hersbach, H. and Hólm, E. V. and Isaksen, L. and Kållberg, P. and Köhler, M. and Matricardi, M. and McNally, A. P. and Monge-Sanz, B. M. and Morcrette, J.-J. and Park, B.-K. and Peubey, C. and de Rosnay, P. and Tavolato, C. and Thépaut, J.-N. and Vitart, F.: The ERA-Interim reanalysis: configuration and performance of the data assimilation system, Quarterly Journal of the Royal Meteorological Society, 137,553-597, doi = 10.1002/qj.828, 2011.

430   De Wachter, E., Barret, B., Le Flochmoën, E., Pavelin, E., Matricardi, M., Clerbaux, C., Hadji-Lazaro, J., George, M., Hurtmans, D., Coheur, P.-F., Nedelec, P., and Cammas, J. P.: Retrieval of MetOp-A/IASI CO profiles and validation with MOZAIC data, Atmos. Meas. Tech., 5, 2843-2857, doi:10.5194/amt-5-2843-2012, 2012.

Duc, H. N., Bang, H. Q., and Quang, N. X.: Modelling and prediction of air pollutant transport during the 2014 biomass

435   burning and forest fires in peninsular Southeast Asia, Environ. Monit. Assess, 188: 106., DOI: 10.1007/s10661-016-5106-9, 2016.

Fioletov, V. E., C. A. McLinden, N. Krotkov, and C. Li : Lifetimes and emissions of SO_2 from point sources estimated from OMI, Geophys. Res. Lett., 42, 1969–1976, doi:10.1002/2015GL063148, 2015.

440

Gabriel, R., Schäfer, L., Gerlach, C., Rausch, T. and Kesselmeier, J.: Factors controlling the emissions of volatile organic acids from leaves of Quercus ilex L. (Holm oak). Atmos. Env., 33, 1347-1355, 1999.

George, M., Clerbaux, C., Hurtmans, D., Turquety, S., Coheur, P.-F., Pommier, M., Hadji-Lazaro, J., Edwards, D. P.,

445   Worden, H., Luo, M., Rinsland, C., and McMillan, W.: Carbon monoxide distributions from the IASI/METOP mission: evaluation with other space-borne remote sensors, Atmos. Chem. Phys., 9, 8317-8330, doi:10.5194/acp-9-8317-2009, 2009.

Giglio, L., van der Werf, G. R., Randerson, J. T., Collatz, G. J., and Kasibhatla, P.: Global estimation of burned area using MODIS active fire observations, Atmos. Chem. Phys., 6, 957-974, doi:10.5194/acp-6-957-2006, 2006.

450

Giglio, L.: MODIS Collection 5 Active Fire Product User's Guide, v2.5, Updated 31 March 2013, 2013.

González Abad, G., Bernath, P. F., Boone, C. D., McLeod, S. D., Manney, G. L., and Toon, G. C.: Global distribution of upper tropospheric formic acid from the ACE-FTS, Atmos. Chem. Phys., 9, 8039-8047, doi:10.5194/acp-9-8039-2009, 2009.

455

Goode, J., Yokelson, R., Ward, D., Susott, R., Babbitt, R., Davies, M., and Hao, W.: Measurements of excess O_3, CO_2, CO, CH_4, C_2H_4, C_2H_2, HCN, NO, NH_3, HCOOH, CH_3COOH, HCHO, and CH_3OH in 1997 Alaskan biomass burning plumes by airborne Fourier transform infrared spectroscopy (AFTIR), J. Geophys. Res., 105, 22147, doi:10.1029/2000JD900287, 2000.

460   Graedel, T., and Eisner, T.: Atmospheric formic acid from formicine ants: a preliminary assessment, Tellus B, 40, 335–339, 1988.

Grosjean, D.: Organic acids in southern California air: ambient concentrations, mobile source emissions, in situ formation and removal processes, Environ. Sci. Technol., 23, 1506–1514, 1989.

465

Grutter, M., Glatthor, N., Stiller, G. P., Fischer, H., Grabowski, U., Höpfner, M., Kellmann, S., Linden, A., and von Clarmann, T.: Global distribution and variability of formic acid as observed by MIPAS-ENVISAT, J. Geophys. Res., 115, D10303, doi:10.1029/2009JD012980, 2010.

470   Hatakeyama, S., Washida, N., and Akimoto, H.: Rate constants and mechanisms for the reaction of hydroxyl (OD) radicals with acetylene, propyne, and 2-butyne in air at 297±2K, J. Phys. Chem., 6, 90, 173–178, 1986.

Hurtmans, D., Coheur, P.-F., Wespes, C., Clarisse, L., Scharf, O., Clerbaux, C., Hadji-Lazaro, J., George, M., and Turquety, S.: FORLI radiative transfer and retrieval code for IASI, J. Quant. Spectrosc. Radiat. Transf., 113, 1391–1408, 475   doi:10.1016/j.jqsrt.2012.02.036, 2012.

Hurst, D. F., Griffith, D. W. T., and Cook, G. D.: Trace gas emissions from biomass burning in tropical Australian savannas. Journal of Geophysical Research, 99(D8), 16441–16456, doi:10.1029/94JD00670, 1994.

480   Justice, C.O., Giglio, L., Korontzi, S., Owens, J., Morisette, J.T., Roy, D., Descloitres, J., Alleaume, S., Petitcolin, F., Kaufman, Y.: The MODIS fire products. Rem. Sens. Environ. 83, 244-262.2002.

Kaskaoutis, D. G., Kumar, S., Sharma, D., Singh, R. P., Kharol, S. K., Sharma, M., Singh, A. K., Singh, S., Singh, A., and Singh, D.: Effects of crop residue burning on aerosol properties, plume characteristics, and long-range transport over 485   northern India, J. Geophys. Res. Atmos., 119, 5424–5444, doi:10.1002/2013JD021357, 2014.

Kawamura, K., Ng, L.-L., and Kaplan, I.: Determination of organic acids (C_1-C_{10}) in the atmosphere, motor exhausts, and engine oils, Environ. Sci. Technol., 19, 1082–1086, 1985.

490   Keene, W. and Galloway, J.: Organic acidity in precipitation of North America, Atmos. Environ., 18, 2491–2497, 1984.

Keene, W. and Galloway, J.: The biogeochemical cycling of formic and acetic acids through the troposphere: An overview of current understanding, Tellus B, 40, 322–334, 1988.

495   Kerzenmacher, T., Dils, B., Kumps, N., Blumenstock, T., Clerbaux, C., Coheur, P.-F., Demoulin, P., García, O., George, M., Griffith, D. W. T., Hase, F., Hadji-Lazaro, J., Hurtmans, D., Jones, N., Mahieu, E., Notholt, J., Paton-Walsh, C., Raffalski, U., Ridder, T., Schneider, M., Servais, C., and De Mazière, M.: Validation of IASI FORLI carbon monoxide retrievals using FTIR data from NDACC, Atmos. Meas. Tech., 5, 2751-2761, doi:10.5194/amt-5-2751-2012, 2012.

500   Krol, M., Peters, W., Hooghiemstra, P., George, M., Clerbaux, C., Hurtmans, D., McInerney, D., Sedano, F., Bergamaschi, P., El Hajj, M., Kaiser, J. W., Fisher, D., Yershov, V., and Muller, J.-P.: How much CO was emitted by the 2010 fires around Moscow?, Atmos. Chem. Phys., 13, 4737-4747, doi:10.5194/acp-13-4737-2013, 2013.

Lee, A., Goldstein, A. H., Kroll, J. H., Ng, N. L., Varutbangkul, V., Flagan, R. C., and Seinfeld, J. H.: Gas-phase products
505   and secondary aerosol yields from the photooxidation of different terpenes, J. Geophys. Res., 111, D17305, doi: 10.1029/2006JD007050, 2006.

Neeb, P., Sauer, F., Horie, O., and Moortgat, G. K.: Formation of hydroxymethyl hydroperoxide and formic acid in alkene ozonolysis in the presence of water vapour, Atmos. Environ., 31, 1417–1423, 1997.
510
Ohara, T., Akimoto, H., Kurokawa, J., Horii, N., Yamaji, K., Yan, X., and Hayasaka, T.: An Asian emission inventory of anthropogenic emission sources for the period 1980–2020, Atmos. Chem. Phys., 7, 4419-4444, doi:10.5194/acp-7-4419-2007, 2007.

515   Ohta, K., Ogawa, H. , and Mizuno, T.: Abiological formation of formic acid on rocks in nature. Appl. Geochem. 15, 91-95, 2000.

Paris, J.-D., Ciais, P., Nedelec, P., Ramonet, M., Belan, B. D., Arshinov, M. Yu., Golitsyn, G. S., Granberg, I., Stohl, A., Cayez, G., Athier, G., Boumard, F. and Cousin, J.-M. : The YAK-AEROSIB transcontinental aircraft campaigns: new
520   insights on the transport of CO_2, CO and O_3 across Siberia. Tellus B, 60, 551–568, doi:10.1111/j.1600-0889.2008.00369.x, 2008.

Paton-Walsh, C., Jones, N. B., Wilson, S. R., Haverd, V., Meier, A., Griffith, D. W. T., and Rinsland, C. P.: Measurements of trace gas emissions from Australian forest fires and correlations with coincident measurements of aerosol optical depth, J.
525   Geophys. Res., 110, D24305, doi:10.1029/2005JD006202, 2005.

Paulot, F., et al..: Importance of secondary sources in the atmospheric budgets of formic and acetic acids, Atmos. Chem. Phys., 11, 1989–2013, doi:10.5194/acp-11-1989-2011, 2011.

530   Pochanart, P., Akimoto, H., Kajii, Y., Potemkin, V. M., and Khodzher, T. V. : Regional background ozone and carbon monoxide variations in remote Siberia/East Asia, J. Geophys. Res., 108(D1), 4028, doi:10.1029/2001JD001412, 2003.

Pommier, M., Law, K. S., Clerbaux, C., Turquety, S., Hurtmans, D., Hadji-Lazaro, J., Coheur, P.-F., Schlager, H., Ancellet, G., Paris, J.-D., Nédélec, P., Diskin, G. S., Podolske, J. R., Holloway, J. S., and Bernath, P.: IASI carbon monoxide

535   validation over the Arctic during POLARCAT spring and summer campaigns, Atmos. Chem. Phys., 10, 10655-10678,
       doi:10.5194/acp-10-10655-2010, 2010.

       Pommier, M., McLinden, C. A., and Deeter, M.: Relative changes in CO emissions over megacities based on observations
       from space, Geophys. Res. Lett., 40, 3766–3771, doi:10.1002/grl.50704, 2013.

540

       Pommier, M., Clerbaux, C., Coheur, P.-F., Mahieu, E., Müller, J.-F., Paton-Walsh, C., Stavrakou, T., and Vigouroux, C.:
       HCOOH distributions from IASI for 2008–2014: comparison with ground-based FTIR measurements and a global
       chemistry-transport model, Atmos. Chem. Phys., 16, 8963-8981, doi:10.5194/acp-16-8963-2016, 2016.

545   R'Honi, Y., Clarisse, L., Clerbaux, C., Hurtmans, D., Duflot, V., Turquety, S., Ngadi, Y., and Coheur, P.-F.: Exceptional
       emissions of NH_3 and HCOOH in the 2010 Russian wildfires, Atmos. Chem. Phys., 13, 4171-4181, doi:10.5194/acp-13-
       4171-2013, 2013.

       Rinsland, C. P., Boone, C. D., Bernath, P. F., Mahieu, E., Zander, R., Dufour, G., Clerbaux, C., Turquety, S., Chiou, L.,
550   McConnell, J. C., Neary, L., and Kaminski, J. W. : First space-based observations of formic acid (HCOOH): Atmospheric
       Chemistry Experiment austral spring 2004 and 2005 Southern Hemisphere tropical-mid-latitude upper tropospheric
       measurements, Geophys. Res. Lett., 33, L23804, doi:10.1029/2006GL027128, 2006.

       Rinsland, C. P., Dufour, G., Boone, C. D., Bernath, P. F., Chiou, L., Coheur, P.-F., Turquety, S., and Clerbaux, C.: Satellite
555   boreal measurements over Alaska and Canada during June–July 2004: Simultaneous measurements of upper tropospheric
       CO, C_2H_6, HCN, CH_3Cl, CH_4, C_2H_2, CH_3OH, HCOOH, OCS, and SF_6 mixing ratios, Global Biogeochem. Cycles, 21,
       GB3008, doi:10.1029/2006GB002795, 2007.

       Rodgers, C. D.: Inverse methods for atmospheric sounding: theory and practice, Ser. Atmos. Ocean. Planet. Phys. 2, World
560   Sci., Hackensack, NJ, 2000.

       Sanhueza, E. and Andreae, M.: Emission of formic and acetic acids from tropical savanna soils, Geophys. Res. Lett., 18,
       1707–1710, 1991.

565   Schreier, S. F., Richter, A., Kaiser, J. W., and Burrows, J. P.: The empirical relationship between satellite-derived
       tropospheric NO_2 and fire radiative power and possible implications for fire emission rates of NO_x, Atmos. Chem. Phys., 14,
       2447-2466, doi:10.5194/acp-14-2447-2014, 2014.

       Sinha, P., P. Hobbs, V., Yokelson, R. J., Bertschi, I. T., Blake, D. R., Simpson, I. J., Gao, S., Kirchstetter, T. W., and
570   Novakov, T.: Emissions of trace gases and particles from savanna fires in southern Africa, J. Geophys. Res., 108, 8487,
       doi:10.1029/2002JD002325, D13, 2003.

       Sinha, P., P. Hobbs, V., Yokelson, R. J., Blake, D. R., Gao, S., and Kirchstetter, T. W.: Emissions from miombo woodland
       and dambo grassland savanna fires, J. Geophys. Res., 109, D11305, doi:10.1029/2004JD004521, 2004.

575

       Srinivas, R., Beig, G., and Peshin S. K. : Role of transport in elevated CO levels over Delhi during onset phase of monsoon,
       Atmos. Env,140, 234-241, http://dx.doi.org/10.1016/j.atmosenv.2016.06.003, 2016.

Stavrakou, T., Müller, J-F., Peeters, J., Razavi, A., Clarisse, L., Clerbaux, C., Coheur, P.-F., Hurtmans, D., and De Mazière, M.: Satellite evidence for a large source of formic acid from boreal and tropical forests, Nat. Geosci., 5, 26–30, doi:10.1038/ngeo1354, 2012.

Tereszchuk, K. A., González Abad, G., Clerbaux, C., Hurtmans, D., Coheur, P.-F., and Bernath, P. F.: ACE-FTS measurements of trace species in the characterization of biomass burning plumes, Atmos. Chem. Phys., 11, 12169-12179, doi:10.5194/acp-11-12169-2011, 2011.

Tereszchuk, K. A., González Abad, G., Clerbaux, C., Hadji-Lazaro, J., Hurtmans, D., Coheur, P.-F., and Bernath, P. F.: ACE-FTS observations of pyrogenic trace species in boreal biomass burning plumes during BORTAS, Atmos. Chem. Phys., 13, 4529-4541, doi:10.5194/acp-13-4529-2013, 2013.

Turquety, S., Hurtmans, D., Hadji-Lazaro, J., Coheur, P.-F., Clerbaux, C., Josset, D., and Tsamalis, C.: Tracking the emission and transport of pollution from wildfires using the IASI CO retrievals: analysis of the summer 2007 Greek fires, Atmos. Chem. Phys., 9, 4897-4913, doi:10.5194/acp-9-4897-2009, 2009.

Vadrevu, K. P., Lasko, K., Giglio, L., and Justice, C.: Vegetation fires, absorbing aerosols and smoke plume characteristics in diverse biomass burning regions of Asia, Environ. Res. Lett., 10, 2371-2379, DOI:10.1039/c4em00307a, 2015.

van der Werf, G. R., Randerson, J. T., Giglio, L., Collatz, G. J., Mu, M., Kasibhatla, P. S., Morton, D. C., DeFries, R. S., Jin, Y., and van Leeuwen, T. T.: Global fire emissions and the contribution of deforestation, savanna, forest, agricultural, and peat fires (1997–2009), Atmos. Chem. Phys., 10, 11707-11735, doi:10.5194/acp-10-11707-2010, 2010.

Viatte, C., Strong, K., Hannigan, J., Nussbaumer, E., Emmons, L. K., Conway, S., Paton-Walsh, C., Hartley, J., Benmergui, J., and Lin, J.: Identifying fire plumes in the Arctic with tropospheric FTIR measurements and transport models, Atmos. Chem. Phys., 15, 2227-2246, doi:10.5194/acp-15-2227-2015, 2015.

Vigouroux, C., Stavrakou, T., Whaley, C., Dils, B., Duflot, V., Hermans, C., Kumps, N., Metzger, J.-M., Scolas, F., Vanhaelewyn, G., Müller, J.-F., Jones, D. B. A., Li, Q., and De Mazière, M.: FTIR time-series of biomass burning products (HCN, C_2H_6, C_2H_2, CH_3OH, and HCOOH) at Reunion Island (21° S, 55° E) and comparisons with model data, Atmos. Chem. Phys., 12, 10367-10385, doi:10.5194/acp-12-10367-2012, 2012.

White, F.: UNESCO/AETFAT/UNSO vegetation map of Africa, scale 1:5,000,000, UNESCO, Paris, 1981.

Whitburn, S., Van Damme, M., Kaiser, J. W., van der Werf, G. R., Turquety, S., Hurtmans, D., Clarisse, L., Clerbaux, C., and Coheur, P.-F.: Ammonia emissions in tropical biomass burning regions: Comparison between satellite-derived emissions and bottom-up fire inventories, Atmos. Environ, 121, 42–54, doi:10.1016/j.atmosenv.2015.03.015, 2015.

Wooster, M. J., Roberts, G., Perry, G. L. W., and Kaufman, Y. J.: Retrieval of biomass combustion rates and totals from fire radiative power observations: FRP derivation and calibration relationships between biomass consumption and fire radiative energy release, J. Geophys. Res., 110, D24311, doi:10.1029/2005JD006318, 2005.

Yokelson, R. J., Bertschi, I. T., Christian, T. J., Hobbs, P. V., Ward, D. E., and Hao, W. M.: Trace gas measurements in nascent, aged, and cloud-processed smoke from African savanna fires by airborne Fourier transform infrared spectroscopy (AFTIR), J. Geophys. Res., 108, 8478, doi:10.1029/2002JD002322, 2003.

625   Yokelson, R. J., Karl, T., Artaxo, P., Blake, D. R., Christian, T. J., Griffith, D. W. T., Guenther, A., and Hao, W. M.: The Tropical Forest and Fire Emissions Experiment: overview and airborne fire emission factor measurements, Atmos. Chem. Phys., 7, 5175-5196, doi:10.5194/acp-7-5175-2007, 2007.

Yokelson, R. J., Christian, T. J., Karl, T. G., and Guenther, A.: The tropical forest and fire emissions experiment: laboratory
630   fire measurements and synthesis of campaign data, Atmos. Chem. Phys., 8, 3509-3527, doi:10.5194/acp-8-3509-2008, 2008.

Yokelson, R. J., Akagi, S. K., Griffith, D. W. T., and Johnson, T. J.: Interactive comment on "Exceptional emissions of NH_3 and HCOOH in the 2010 Russian wildfires" by Y. R'Honi et al., Atmos. Chem. Phys. Discuss., 12, C11864–C11868, 2013.

635

640

645

650

655

660

665

670

Tab. 1 Correlation coefficients between the HCOOH total columns and the CO total columns measured by IASI for the period between 2008 and 2014 over the 7 studied regions. Each IASI data is selected in an area of 50 km around the MODIS fire hotspot and up to 5h after the time recorded for each fire. The number of fires characterized by HCOOH and CO total columns is given in parenthesis.

	AMA	AUS	IND	SEA	SAF	NAF	SIB
r	0.78	0.63	0.53	0.84	0.78	0.58	0.65
	(13342)	(1525)	(1641)	(1865)	(12227)	(21139)	(22353)

Tab. 2 As Tab.1 but with only MODIS fire hotspot having a surface wind speed lower than 1.44 m/s.

	AMA	AUS	IND	SEA	SAF	NAF	SIB
r	0.79	0.65	0.65	0.86	0.80	0.53	0.72
	(4580)	(93)	(340)	(528)	(895)	(1095)	(2097)

675

680

685

690

695

700

705

710

715

Tab. 3 Enhancement ratio to CO (mol/mol) for HCOOH with its standard deviation compared to enhancement ratios and emissions ratios reported in the literature for the seven studied regions.

Region	Enhancement Ratio to CO (mol/mol) – this work	Enhancement Ratio to CO (mol/mol) found in literature	Emission Ratio to CO (mol/mol) found in literature	Instrument used
AMA	$7.3\times10^{-3} \pm 0.08\times10^{-3}$	$5.1\times10^{-3} \pm 1.5\times10^{-3}$ (González Abad et al., 2009)*		ACE-FTS
		$6.7\times10^{-3} \pm 2.1\times10^{-3}$ (Chaliyakunnel et al., 2016)		TES
AUS	$11.1\times10^{-3} \pm 1.37\times10^{-3}$	$4.5\times10^{-3} \pm 5.1\times10^{-3}$ (Chaliyakunnel et al., 2016)		TES
		$21.0\times10^{-3} \pm 10.0\times10^{-3}$ (Paton-Walsh et al., 2005)*		Ground-based FTIR
IND	$6.8\times10^{-3} \pm 0.44\times10^{-3}$	None	-	
SEA	$5.8\times10^{-3} \pm 0.15\times10^{-3}$	None	-	
NAF	$4.0\times10^{-3} \pm 0.19\times10^{-3}$	$2.8\times10^{-3} \pm 0.4\times10^{-3}$ (Chaliyakunnel et al., 2016)		TES
SAF	$5.0\times10^{-3} \pm 0.13\times10^{-3}$	$2.6\times10^{-3} \pm 0.3\times10^{-3}$ (Chaliyakunnel et al., 2016)		TES
		$4.6\times10^{-3} \pm 0.3\times10^{-3}$ (Vigouroux et al., 2012)		Ground-based FTIR
		5.1×10^{-3} (Coheur et al., 2007)		ACE-FTS
		$11.3\times10^{-3} \pm 7.6\times10^{-3}$ (Rinsland et al., 2006)*		ACE-FTS
			$5.9\times10^{-3} \pm 2.2\times10^{-3}$ (Yokelson et al., 2003)	Airborne FTIR
			$5.1-8.7\times10^{-3}$ (Sinha al., 2003)	Airborne FTIR
SIB	$4.4\times10^{-3} \pm 0.09\times10^{-3}$	$0.77-6.41\times10^{-3}$ (Tereszchuk et al., 2013)		ACE-FTS
		$2.69-15.93\times10^{-3}$ (Viatte et al., 2015)		Ground-based FTIR
		$10.0-32.0\times10^{-3}$ (R'honi et al., 2013)		IASI

720   * Their "emission ratios" are requalified as enhancement ratios in this study since their ratios were not measured at the origin the fire emission but at high altitudes and/or further downwind of the fires.

725

Tab. 4 Enhancement ratio to CO (mol/mol) for HCOOH with its standard deviation compared to emission ratios calculated from emission factors given in literature for the seven studied regions. For the calculation of these emission ratios, the emission factors for CO for the corresponding fuel type given in Akagi et al. (2011) are used. Emission ratios to CO (mol/mol) for HCOOH calculated from the emission factors for HCOOH given in Akagi et al. (2011) for the corresponding fuel type are also provided.

Region	Enhancement Ratio to CO (mol/mol) – this work	Emission Ratio to CO (mol/mol) calculated from EF_{HCOOH} given in literature and using EF_{CO} from Akagi et al. (2011)	Instrument used
AMA	$7.3\times10^{-3} \pm 0.08\times10^{-3}$	1.8×10^{-3} – Tropical forest (Yokelson et al., 2007 ; 2008)* 2.7×10^{-3} – Savanna (Yokelson et al., 2007 ; 2008)* 2.0×10^{-3} – Savanna (Akagi et al., 2011) 5.2×10^{-3} – Tropical forest (Akagi et al., 2011)	Airborne FTIR (Yokelson et al., 2007) ; laboratory (Yokelson et al., 2008) catalogue
AUS	$11.1\times10^{-3} \pm 1.37\times10^{-3}$	2.0×10^{-3} – Savanna (Akagi et al., 2011)	catalogue
IND	$6.8\times10^{-3} \pm 0.44\times10^{-3}$	2.7×10^{-3} – Extratropical forest (Akagi et al., 2011) 6.0×10^{-3} – Cropland (Akagi et al., 2011)	catalogue
SEA	$5.8\times10^{-3} \pm 0.15\times10^{-3}$	2.0×10^{-3} – Savanna (Akagi et al., 2011) 2.7×10^{-3} – Extratropical forest (Akagi et al., 2011) 6.0×10^{-3} – Cropland (Akagi et al., 2011)	catalogue
NAF	$4.0\times10^{-3} \pm 0.19\times10^{-3}$	2.0×10^{-3} – Savanna (Akagi et al., 2011)	catalogue
SAF	$5.0\times10^{-3} \pm 0.13\times10^{-3}$	3.3×10^{-3} – Tropical forest (Sinha et al., 2004)** 4.8×10^{-3} – Savanna (Sinha et al., 2004)** 4.1×10^{-3} – Tropical forest (Yokelson et al., 2003) 6.0×10^{-3} – Savanna (Yokelson et al., 2003) 13×10^{-3} – Tropical forest (Rinsland et al., 2006) 19.2×10^{-3} – Savanna (Rinsland et al., 2006) 2.0×10^{-3} – Savanna (Akagi et al., 2011) 5.2×10^{-3} – Tropical forest (Akagi et al., 2011)	Airborne FTIR Airborne FTIR ACE-FTS catalogue
SIB	$4.4\times10^{-3} \pm 0.09\times10^{-3}$	2.7×10^{-3} – Boreal forest (Akagi et al., 2011)	catalogue

* The EF_{HCOOH} were corrected based on the comment from Yokelson et al. (2013) (EF_{HCOOH} used: 0.281 for Yokelson et al. (2007); 0.2767 for Yokelson et al. (2008)).

** The mean of both EF_{HCOOH} values provided in Sinha et al. (2004) were used for our $EmR_{HCOOH/CO}$ calculation.
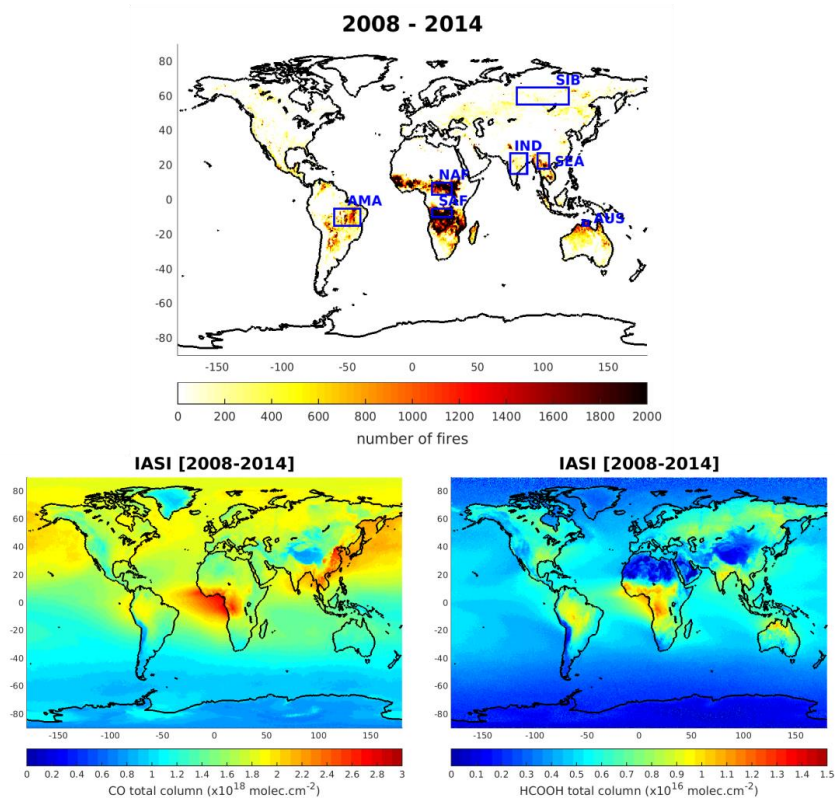
Figure 1: Top: Number of MODIS fire hotspots with a confidence percentage higher or equal to 80%, averaged on a 0.5°×0.5° grid, for the period between 2008 and 2014. The blue boxes are the regions studied in this work. Bottom: The IASI CO total columns distribution (left) and the IASI HCOOH total columns distribution (right), for the same period and averaged on the same grid.
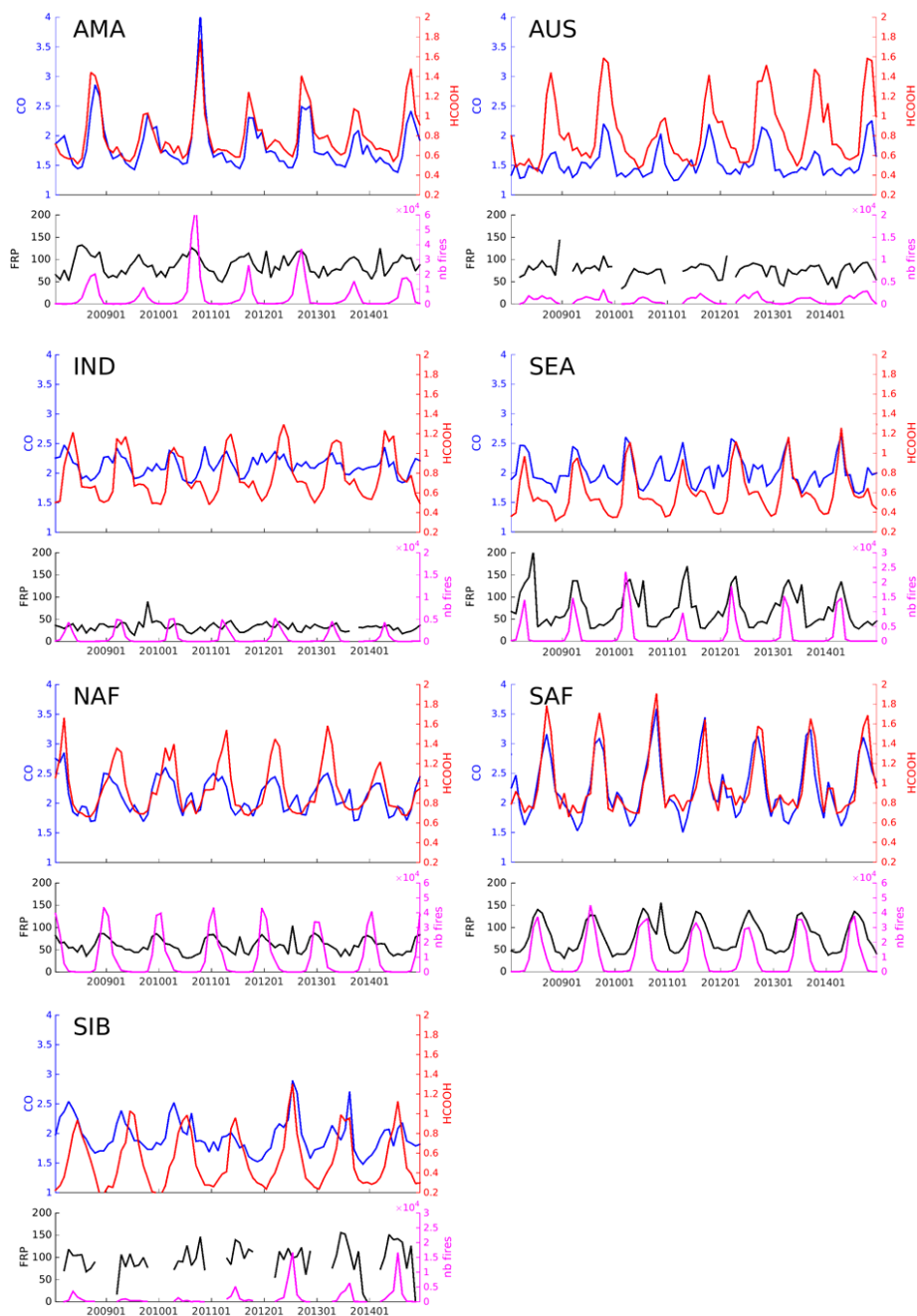
750 **Figure 2: Time-series from 2008 to 2014 of the monthly means of IASI CO (blue) and HCOOH (red) total columns in 10^{18} molec/cm^2 and in 10^{16} molec/cm^2, respectively, FRP (black) in MegaWatts and the number of fires (magenta) from MODIS over the seven regions (AMA=Amazonia, AUS=Australia, IND = India, SEA = Southern East Asia, NAF= Northern Africa, SAF= Southern Africa, SIB= Siberia).**
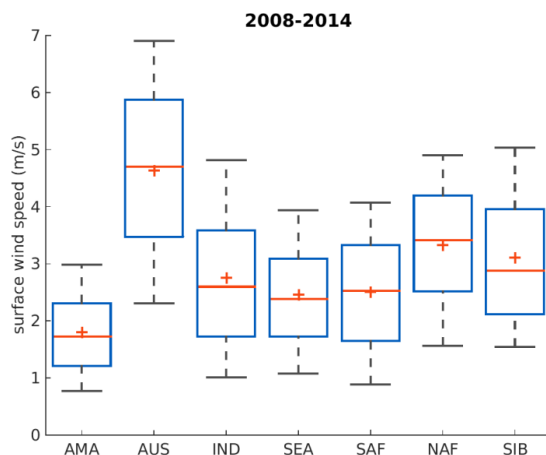
Figure 3: Box and whisker plots showing mean (red central cross), median (red central line), and 25th and 75th percentile (blue box edges) of surface wind speed for each MODIS hotspot over the studied regions (AMA=Amazonia, AUS=Australia, IND = India, SEA = Southern East Asia, NAF= Northern Africa, SAF= Southern Africa, SIB= Siberia).The whiskers encompass values from 25th-1.5×(75th-25th) to the 75th+1.5× (75th-25th). This range covers more than 99% of a normally distributed data set.
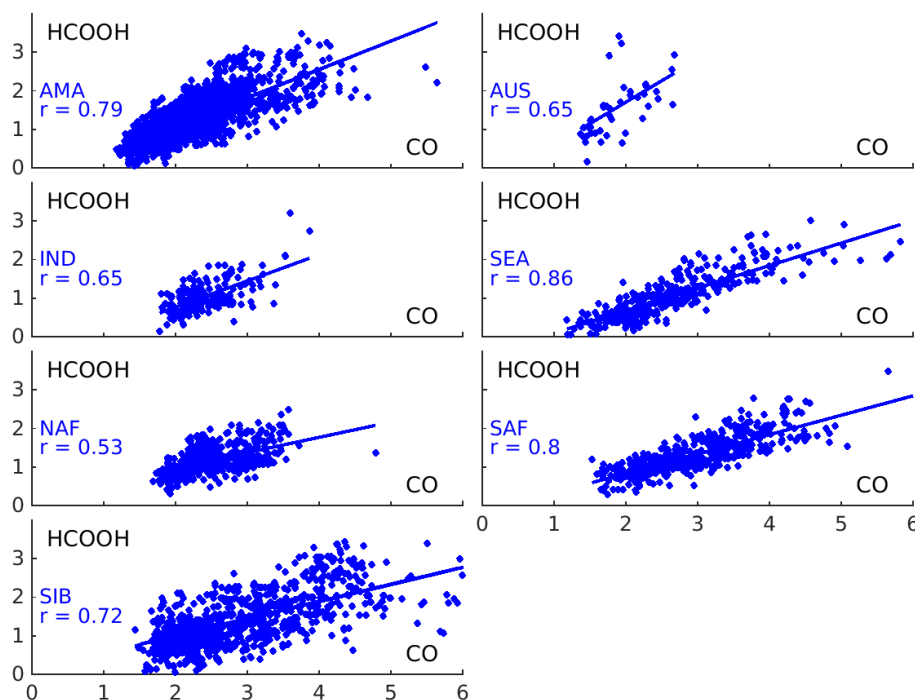
Figure 4: Scatterplots between the IASI fire-affected HCOOH total columns (in 10^{16} molec/cm^2) and the CO total columns (in 10^{18} molec/cm^2) over the seven regions (AMA=Amazonia, AUS=Australia, IND = India, SEA = Southern East Asia, NAF= Northern Africa, SAF= Southern Africa, SIB= Siberia).The linear regression is represented by the blue line and the correlation coefficient is also provided for each region.